Long time extrapolation of DEM with heat conduction in a moving granular medium

Clara Haydar, Sylvain Martin, Olivier Bonnefoy

Long time extrapolation of DEM with heat conduction in a moving granular medium

Clara HAYDAR[a], Sylvain MARTIN[a,*], Olivier BONNEFOY[a]

[a] *Mines Saint-Etienne, Univ Lyon, CNRS, UMR 5307 LGF, Centre SPIN, F - 42023 Saint-Etienne France*

Abstract

This paper presents a novel approach for extrapolating DEM simulations of heat transfer over a long period of time. This method is an extension of a previously published algorithm for granular motion extrapolation, introducing heat transfer. The main idea is to perform a short-term DEM simulation for one period and then apply a conductive heat transfer extrapolation algorithm. This strategy is tested over a pilot-scale rotating drum. The outcomes of standard and extrapolated DEM simulations are compared. The results are very similar while the computational time is reduced by a factor greater than 100.

Keywords: Granular system, DEM, heat transfer, long time extrapolation

1. Introduction

DEM[1] is an effective simulation tool for granular systems Cundall & Strack (1979). Powder rheology is guided through the contacts occurring between the particles and it is the method that takes into account the physics of collisions between particles. DEM can be applied to many industrial processes including those in the chemical, building and pharmaceutical industries Muzzio et al. (2004). Even with the abundance of particles-containing systems in nature and industrial processes, a fundamental understanding of heat transfer between the particles during contact is missing Hartmanshenn et al. (2019). However, the

*sylvain.martin@emse.fr

[1] Discrete Element Method

comprehension of such phenomena is essential in order to predict the intrinsic properties of the particles during collision Fry et al. (2019). Yet, due to the complexity of the interactions between the solid particles, these models are difficult to be applied, particularly because simulating the mechanical behavior of granular materials including heat transfer can be computationally expensive Liu et al. (2021). Many modeling methods are proposed in the literature for simulating heat transfer in granular media. One of them is to use coarse-graining as in Saruwatari & Nakamura (2022) and De et al. (2022). This approach enables the representation of a large number of small particles by a small number of macroscopic particles, explained in details in Peters et al. (2023). In Saruwatari & Nakamura (2022), the potency of the coarse-graining technique is demonstrated for simulating heat transfer in rotary kiln reactor. Another option is to use a multi-scale modeling approach that consists of coupling a continuum method with DEM for the simulation of heat conduction in granular materials Zhang et al. (2011). While Zhao et al. (2020) coupled FEM[2] with DEM to simulate the thermo-mechanical response of a granular medium. A different strategy is to employ a thermal DEM approach known in literature as TDEM[3] as in Feng et al. (2008, 2009). The TDEM is considered as a variation of the DEM applied only for heat transfer problems. It enables the representation of a large granular system as a combination of different individual particles affected by different temperature boundary conditions. This enables the determination of the temperature distribution of the particles in the system over time Kiani-Oshtorjani & Jalali (2019) . However, all of the previously stated method share a major limitation which is the high computational cost. Therefore, the aim of our work is to challenge the limits especially those linked to the reduction of time scales Bertrand et al. (2005). For this paper, we will shed light on the reduction of time of DEM for simulating heat transfer in granular media. Physical time is always

[2]Finite Element Method
[3]Thermal Discrete Element Method

considered as the biggest challenge for numericians. Knowing that the parallelizing can give a partial gain of computation for the high number of particles, yet the time variable cannot be parallelized easily. Simulating one million of particles for one hour is still complicated. In order to face this challenge, many research teams found that the idea of pseudo-periodicity for granular process can decrease drastically the duration of numerical simulation. The first idea concerning **time extrapolation** was proposed by Doucet et al. (2008) by using a statistical approach based on Markov process. Then, the team of T. Lichtenegger has introduced the notion of recurrence CFD[4] Pirker & Lichtenegger (2018); Lichtenegger & Pirker (2016); Lichtenegger et al. (2019). It is a method based on the Poincaré's recurrence, which allows the long time extrapolation of fluid/granular flows. Another solution based on an extrapolation algorithm has been proposed previously by a research in our lab Bednarek et al. (2019), the major advantage of which is to be very simple. The latter method was reproduced by Siegmann et al. (2021) and Bauer et al. (2022). Siegmann et al. (2021) applied this method for continuous processes to extrapolate DEM results in the pharmaceutical industry and the extrapolated results showed a good agreement with full DEM results. Whereas Bauer et al. (2022) used time extrapolation method for SPH[5] flow simulations over twin screw extruders. This method led to a CPU[6] time gain of a factor of 10^5 with an accurate representation of mixing kinetics. However, the main limit of the method is that it uses the pseudo periodic behavior of processes, but since most of powder processes are pseudo periodic, these models are still very useful and promising. Hence, it is possible today to extrapolate DEM simulation for long time but it concerns only processes for which there is no need to model phenomena on physical particle scale. Nevertheless, **none of the approaches are able, up to now, to take into account local phenomena on the real particle scale like heat conduc-**

[4]Computational Fluid Dynamics
[5]Smoothed Particle Hydrodynamics
[6]Central Processing Unit

tion. In his approach, Lichtenegger et al. (2016) proposes a newly first method that enables obtaining the transfers inside fluidized beds. However, his method does not take into account collisions, indeed the particles are represented with passive tracers Lichtenegger (2020). Therefore, in this paper we present a new method which consists in an extension for the existing method developed by Bednarek et al. (2019) to heat transfer by conduction in granular media, taking into account particle-particle collisions.

2. Materials and Method

In this part, the numerical method will be presented along with the heat extrapolation algorithm. We need to mention that the novel method is simple and straightforward; it consists as a foundation for further research about time extrapolation simulations.

2.1. DEM model

DEM is a technique that enables the simulation of the behavior of separate particles in interaction under certain circumstances. Contrary to the continuum approach, the DEM approach considers the system's particle flow as discrete particles. It is used to calculate the behavior of the particles, their positions and the forces of collisions between them Huang & Kuo (2018). Particle's trajectory is then obtained by Newton's second law. The DEM model in this study is based on the soft-sphere approach Yazdani & Hashemabadi (2020), which allows for particles overlap as well as particles-boundary overlap. The contact forces due to collisions are calculated by the non-linear spring-dashpot Hertz-Mindlin model, which is detailed in Zhu et al. (2007). The DEM with heat transport will be described using the following steps in the algorithm 1.

A linear heat transfer model between two particles was used based on applying the one dimensional heat transfer equation by conduction. To obtain the heat transfer due to particle-particle conduction, the transport equation is influenced by many parameters such as temperature of the material, the heat

Algorithm 1: General algorithm for DEM along with heat transfer.

for $t = 0 \rightarrow t_{max}$ **do**

- Establish the contact list between the particles and detect changes with previous one;
- For each particle and each contact, compute the force using contact law;
- For each particle and each contact, compute the conductive heat flux using Fourier's law;
- For each particle, sum all forces and heat fluxes;
- Compute the new particles temperature through energy balance;
- Compute the new particles position through Newton's 2nd law;

capacity and the heat transfer coefficient. Heat flux Q_{ij} due to particle-particle collision is calculated using Equation 1 where T_i and T_j are respectively the temperatures of the particles and H_{ij} is the conductance between the particles.

$$Q_{ij} = H_{ij}(T_i - T_j) \tag{1}$$

Modeling granular material will be achieved with the use of LIGGGHTS,[7] an open-source software package Kloss et al. (2012). Based on the heat equations developed in the software, the heat transfer coefficient known as the conductance between particle i and particle j will be obtained by the Equation 2 where K_{ij} is the thermal conductivity and a_{ij} is the area of contact between i and j:

$$H_{ij} = \frac{4K_iK_j}{K_i + K_j}\sqrt{(a_{ij})} \tag{2}$$

And since the particles taken are identical K_i is equal to K_j, hence Equation 1 is simplified to Equation 3:

$$Q_{ij} = 2K_{ij}\sqrt{(a_{ij})}(T_i - T_j) \tag{3}$$

[7] LAMMPS Improved for General Granular and Granular Heat Transfer Simulations

On the other hand, the temperature change for a particle i can be calculated using Equation 4 where $\sum(Q_i)$ is the sum of all heat fluxes involving particle i and $\rho_i C_i V_i$ is the thermal capacity of particle i as in Peng et al. (2020).

$$\frac{dT_i}{dt} = \frac{\sum(Q_i)}{\rho_i C_i V_i} \tag{4}$$

The following simple ordinary differential equation represents the final equation that describes the evolution of the temperature for a given particle i in contact with different particles j:

$$\frac{dT_i}{dt} = \frac{\sum_i 2K_{ij}\sqrt{(a_{ij})}(T_i - T_j)}{\rho_i C_i V_i} \tag{5}$$

For our case of study, $Biot^* = \frac{2K_{ij}r_c}{K_{ij}A_p/r_p} = \frac{2r_c}{\Pi r_p}$, with r_c is the contact radius between the two particles, A_p is the cross-sectional area of the particle and r_p is the particle's radius.The dimensionless group $Biot^*$ refers to the ratio of heat conduction transferred from one particle to the other over the heat conduction inside the particle as in Gui et al. (2013) and Vargas & McCarthy (2001). $r_c = r_p - 0.5 * \Delta_n$ is obtained using LIGGGHTS. Since $Biot^* << 1$, thus the heat conduction within the particle can be neglected in comparison with the conduction between the particles Beaulieu et al. (2021); Kiani-Oshtorjani et al. (2022).

The newly presented approach is for heat transport extrapolation in granular systems. The approach is an extension of the pairing algorithm proposed by Bednarek et al. (2019). More precisely, it consists of a combination between the pairing algorithm along with an implementation of scalar transport for conductive heat transfer. The pairing algorithm enables the extrapolation of granular motion for DEM results, at a very low computational cost, from one period of time over a longer period for any pseudo-periodic process. The previous method is explained in details in Bednarek et al. (2019). The new method is based on the idea that whatever happening during a period will be reccuring. This mean that using the data obtained from the normal DEM simulation for one period on the microscopic level will enable the acquisition of what is happening over a long period by the means of paired particles. The details to get the paired

particles are found in Bednarek et al. (2019), but physically speaking the paired particles refers to the particles connected by a relation which is, here, a bijective function f_{ext}.

$$f_{ext} = \left| \begin{array}{c} [1 \to N] \to [1 \to N] \\ j \to i = f_{ext}(j) \end{array} \right. \tag{6}$$

The function f_{ext} minimizes the sum of the euclidean distance between the paired particles. If particle i is paired with particle j then the position of i at t_2 is obtained by the following equation: $\vec{x}_i(t_2) = \vec{x}_j(t_1)$.

Some assumptions are required for the implementation of this method:

- The system studied should reach a state of pseudo-periodicity which is described in Siegmann et al. (2021). However, since many processes are pseudo-periodic, the application of the method is allowed for a wide range of systems.
- The particle's size is identical Bednarek et al. (2019)
- The void between the particles which, in real systems, is filled with an interstitial fluid mostly air is ignored Chaudhuri et al. (2006)
- The collisions are treated by apparition order which means that the simultaneous contacts of a particle are treated one after the other and the collisions detected at the same time are also processed one after the other as in the output from the DEM simulation.

The first two previously stated conditions are common with the pairing algorithm and this is due to the use of the same algorithm as a basis of our work. However all of these conditions are soft conditions since they do not affect the execution of the extrapolation algorithm. It should be noted that in this preliminary study, the aim is to show the ability of the new algorithm to speed-up granular flow simulations. Hence for simplicity sake, collision area is taken as a constant parameter a_{ij} but the code already includes the calculation of a_{ij} from standard DEM results.

This section will be divided into 3 parts as in the flowchart Figure 1 that refers to the workflow.

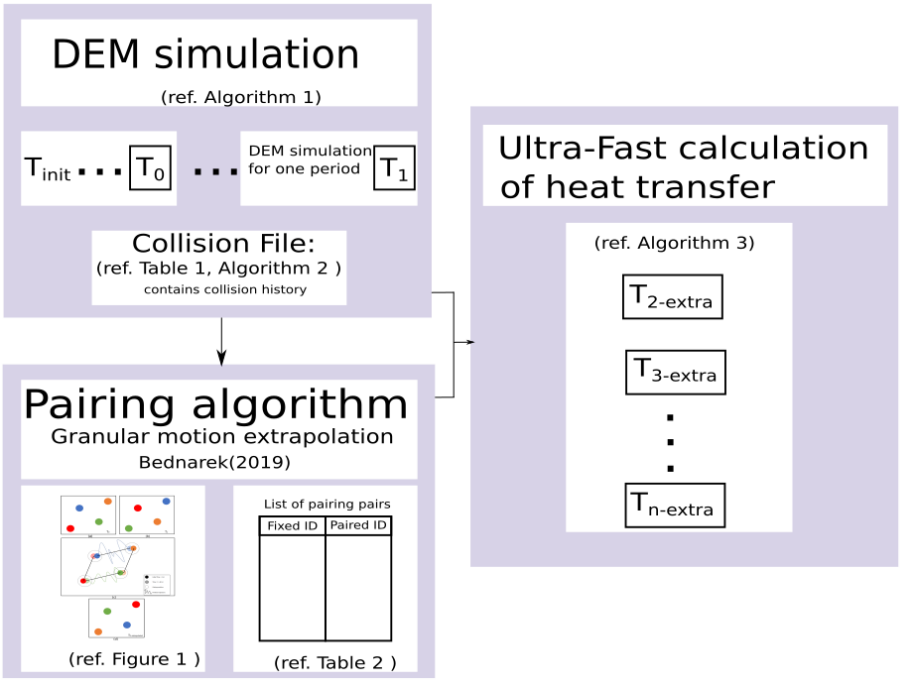

Figure 1: Flowchart of heat extrapolation algorithm.

2.1.1. DEM data

DEM simulations are performed until t_1. It is significant to point out that the DEM simulation should reach a steady state at t_0. In the framework of the extrapolation, all the collisions between t_0 and t_1 are saved and sorted in apparition order. The list of contacts along with its duration and the area of collisions are saved in a table. The final structure of the contact list table is stocked as shown in Table 1.

Since the collision properties between t_0 and t_1 are stored, high memory is required. To solve this limitation, collision sampling is employed. Two parameters are introduced; the first is Δt_c^{max}, the maximum collision time in seconds, which is a maximum imposed collision duration for two particles in contact.

Table 1: Structure of the saved information of the extrapolation for the collisions.

Index	Fixed ID	Fixed ID	t_{init}	m	$\sqrt{(a_{ij})}$
1	5	8	t_0	10.	$8.8e^{-3}$
2	10	6	...	...	...
...	...	...	...	...	...
x	i	j	starts at $t_{init(ij)}$ for $\Delta t_c = 25\ s$ for $\Delta t_c^{max} = 10\ s$		
x	i	j	$t_{init(ij)}$	10.	$7.8e^{-5}$
$x+1$	i	j	$t_{init(ij)} + 10$	10.	...
$x+2$	i	j	$t_{init(ij)} + 20$	5.	...
x	i	j	starts at $t_{init(ij)}$ for $\Delta t_c = 25\ s$ for $\Delta t_c^{max} = 20\ s$		
x	i	j	$t_{init(ij)}$	20.	$7.8e^{-5}$
$x+1$	i	j	$t_{init(ij)} + 20$	5.	...
...	...	...	...	...	...
$nb_{collisions}$-1	...	...	...	...	...
$nb_{collisions}$	...	...	t_1	...	...

And, the second is a sampling factor n, identified using statistical analysis by showing how much time the collision pairs remain in contact. Both of the previously stated parameters aim to reduce the size of the collision table. Δt_c^{max} is an optimization variable that enables us to adjust the size of the output file and the times of operations executed. n enables us to conclude the timesteps' frequency, thus not saving every single timestep, instead saving every n timesteps if the minimum collision duration is n timesteps. The two lines for x^{th} collision in the Table 1 in gray color represent the same phenomenon: a collision between particles i and j that lasts for $\Delta t_c = 25$ seconds. As it can be seen, this collision can be interpreted in two ways: if $\Delta t_c^{max} = 10$ seconds then the output will divided in three rows (the collision will be seen as three different collisions that last for $10 + 10 + 5$), while if $\Delta t_c^{max} = 20$ seconds, the output will be two rows (two collisions $20 + 5$). This will reduce the size of the output file and the time of operations for the numerical calculation. Note that the gray line in Table 1 will not be seen in the final output file, it only serves for detailed explanation. The general algorithm for collision splitting is presented in algorithm 2. It is considered as a refining method to improve the speed of the simulations. It

takes an input, the total collision duration (Δt_c), and compare it to the imposed collision duration (Δt_c^{max}). If Δt_c is less than Δt_c^{max} then m, the single collision duration in Table 1 is equal to Δt_c. Else if it is higher, the collision is splitted into several lines. The number of lines is equal to the floor of $\frac{\Delta t_c}{\Delta t_c^{max}}$ (floor is the function that converts the floating number to the smaller integer (2.7 to 2)) and the last line will be the remainder of the same fraction. Eventually, the algorithm 2 is an external tool that shows how the input table for the extrapolation was handled. It serves only for optimization purpose and for the seek of bigger gain and reduction of the computational time. The extrapolation algorithm can be performed without this algorithm but will need more memory and computational time.

Algorithm 2: Collision splitting algorithm .

```
for k = 1 → nb_collisions do
    if Δt_c ≤ Δt_c^max then
        m = Δt_c;
    else
        for i = 1 → floor(Δt_c / Δt_c^max) do
            m_i = Δt_c^max;
        m_{i+1} = Δt_c modulo(Δt_c^max);
```

2.1.2. Granular motion extrapolation

In Table 1, the fixed ID, represents the identifier of the particles for which the collisions were recorded between t_0 and t_1 during the DEM simulation. These same collisions will be reproduced by the paired particles during the extrapolation steps obtained using the extrapolation function f_{ext}. Figure 2a and Figure 2b illustrate the two states at t_0 and t_1 , which are subsequently superposed to indicate the paired particles. The latter are shown inside the dashed black circles in Figure 2c i.e. for a deeper explanation about f_{ext} refer to Bednarek et al. (2019) article. For the example presented in Figure 2, the pairs

Table 2: List of paired particles.

Fixed ID	Paired particle ID
Red	Blue
Blue	Orange
Orange	Green
Green	Red

of paired particles are shown in Table 2, and the new position (extrapolated) of the particles is shown in Figure 2d.

2.1.3. Heat transfer extrapolation

Based on the presented Equation 5, the newly developed algorithm will calculate the new temperature for the particle i by calculating the sum of the temperature change due to the particles in collisions with i.

In other terms, the temperature of a given particle i at t_2 will be obtained through the heat conduction equation by using the history of the collisions that particle i has experienced. The table of contacts is then traversed for each extrapolation. The temperature of the particles paired with i and j are updated as the collisions with i and j occur. It is simply a matter of numerically integrating the Equation 5.

The objective here is not to aim for extreme precision but to limit the number of operations as much as possible. On the other hand, the stability of the scheme must be guaranteed. The idea is therefore to use a single time step equal to the duration of the collision. As used in the DEM software, an explicit numerical scheme is also employed. Hence, the condition of Courant–Friedrichs–Lewy CFL[8] less than 1 must be checked to assure the convergence of the explicit scheme. This condition is respected if the $m < \frac{\rho_i C_i V_i}{2K_{ij}\sqrt{a_{ij}}}$ indicating that $m <$

[8]Courant Friedrichs Lewy

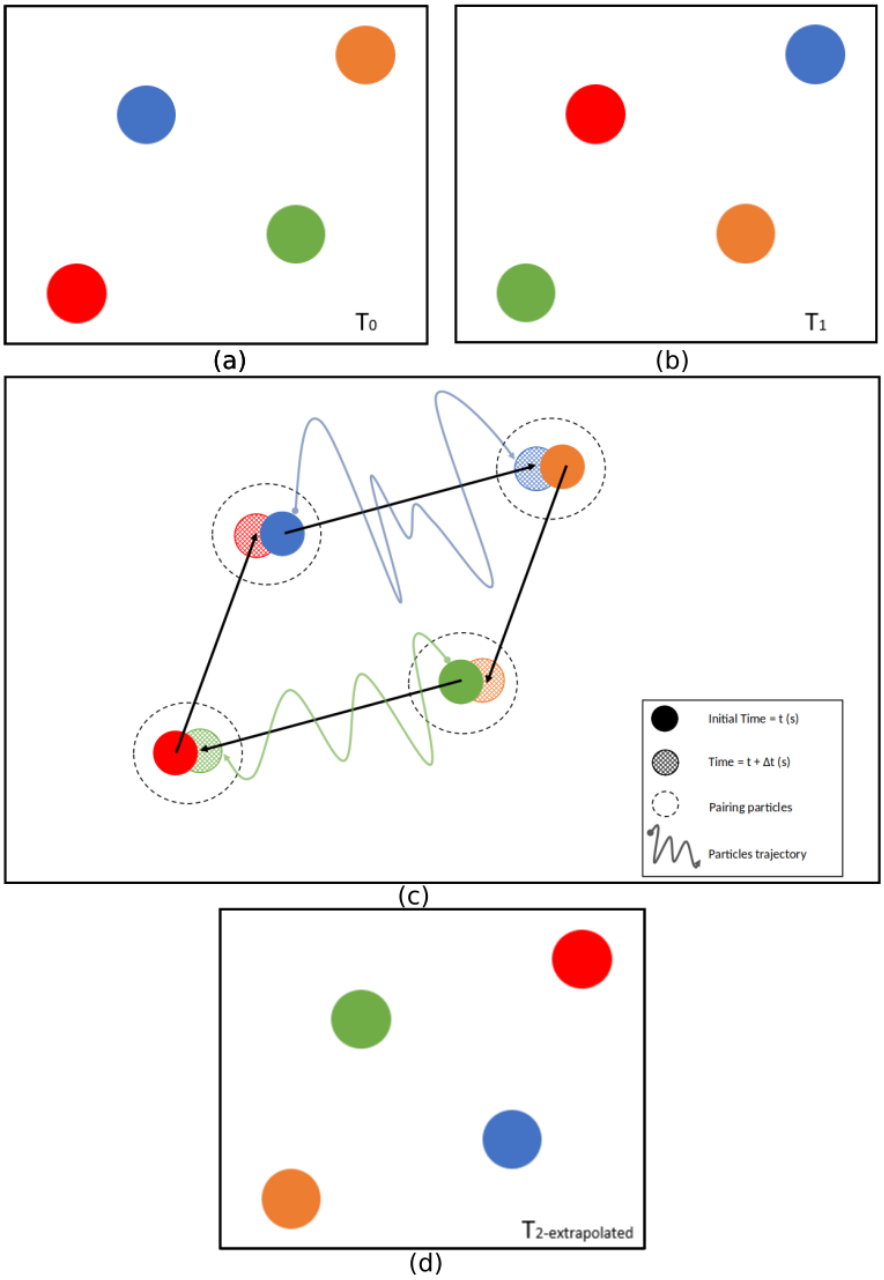

Figure 2: (a) Particles positions at t_0 (b) Particles positions at t_1 (c) Pairing algorithm concept (d) Particles new extrapolated positions at $t_2(extrapolated)$.

$\Delta t_{critical}$.

Then, for a particle i in contact with a particle j, the temperature at the end of the collision $\{T_i^f, T_j^f\}$ is obtained by solving the following system :

$$T_i^f = {T_i}^{t_{ini}} - \frac{Q_{ij}m}{\rho_i C_i V_i} \tag{7}$$

$$T_j^f = {T_j}^{t_{ini}} + \frac{Q_{ij}m}{\rho_i C_i V_i} \tag{8}$$

It should be noted that the couple $\{T_i^f, T_j^f\}$ is not physically equivalent to the temperature of the particles i and j at the final instant of the collision $\{T_i^{t_{ini}+m}, T_j^{t_{ini}+m}\}$.

Indeed, the collisions are treated by order of occurrence. The simultaneous contacts of a particle will be processed one after the other. The contacts detected at the same time are also processed one after the other.

Finally, the conduction transfer extrapolation algorithm is given in the algorithm 3.

Algorithm 3: General algorithm for the extrapolation of heat transfer by conduction.

for $p = 1 \rightarrow nb_{collisions}$ **do**

- Read $i(p)$ in Table 1;
- Read $j(p)$ in Table 1;
- Define $k = f_{ext}(i)$ with respect to pairing algorithm;
- Define $l = f_{ext}(j)$ with respect to pairing algorithm;
- Update by solving T_k^f, T_l^f by solving Equation 7 and Equation 8;

2.2. Rotative drum/Simulation Setup

In granular material, heat transfer can be generated through three different forms: conduction, convection and radiation Nguyen et al. (2014). In this paper, only the heat transfer during particle-particle collisions by conduction will be

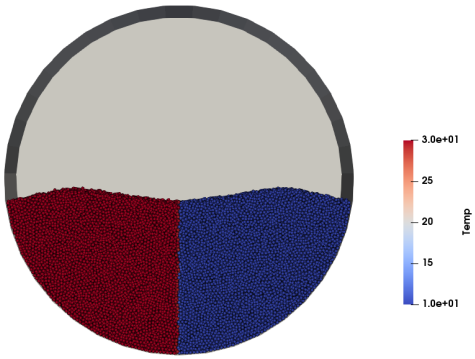

t_{init}

Figure 3: Two halves of particles in rotating drum.

taken into account Gui et al. (2013). Radiation and convection will be neglected as in Chaudhuri et al. (2006). In a rotating kiln, there are two sorts of heating techniques: direct and indirect. Direct heating entails infusing a hot fluid that has undergone a chemical reaction to raise its temperature Herz et al. (2012). The indirect one is caused by increasing the temperature of the drum's casing. In our research, the example that will be employed is the one of a rotating drum containing two halves of particles, with the first half being hot and the other half being cold as shown in Figure 3. Note that the new method works for any heating type or application.

Table 3 and Table 4 show the characteristic parameters used for the simulation. The code can be requested for free on the git repository: code source.

3. Results and discussion

The previously proposed method has been applied over the mixing process of particles in a rotating drum. Many scenarios are tested and the impact of numerous parameters is investigated. Results from standard and extrapolated

Table 3: DEM Parameters.

Parameter	Type	Value
Number	Particles	80000
Radius(r^*)	Particles	0.005 mm
Friction coefficient	Particle-Particle	0.3
	Particle-Wall	0.5
Rolling Friction coefficient	Particle-Particle	0.002
	Particle-Wall	0.002
Restitution coefficient	Particle-Particle	0.2
	Particle-Wall	0.2
Poisson ratio	Particle	0.3
	Wall	0.3
Young Modulus	Particle	$1e^7$ Pa
	Wall	$1e^7$ Pa
Density (ρ_i)	Particles	2500 Kg/m^3
Rotational speed (ω)	Drum	5 s per revolution

Table 4: Heat Transfer Parameters for half cold-half hot.

Parameter	Value	Unit
Initial Temperature of the right subdomain (T)	10	K
Initial Temperature of the left subdomain (T)	30	K
Thermal conductivity (K_{ij})	100	W/(m. K)
Thermal capacity (C_i)	840	J/K

DEM are compared and assessed. All the results shown as temperature profiles are obtained using Paraview.

3.1. Reference case

The reference case that will be presented here is described in details in the preceding section while taking into account all what happens between the two extrapolation instants ($n = 1$) in the Equation 7 and Equation 8. Note that the maximum collision duration is fixed to $\Delta t_c^{max} = 0.001$ seconds which corresponds to 10 DEM time steps. Considering the pairing, after packing the particles, the drum rotates for one rotation before selecting the initial time of the pairing t_0. The initial time of extrapolation, t_1, is then selected when half a rotation has been completed as in Figure 4. Here τ, the extrapolation period, is equal to a rotation. It should be mentioned that a pseudo-periodic state has already been seen by looking at the interface of the particles that is not changing. The outcomes of the standard and extrapolated DEM are then visualized as shown in Figure 5 and Figure 6. In Figure 7, in red, the average temperature of the hot particles DEM $\overline{T_{hot}}$ is compared with the extrapolated average temperature of the same hot particles *extra* $\overline{T_{hot}}$ as in Wang et al. (2019). Analogically, in blue, the standard average temperature DEM $\overline{T_{cold}}$ and the extrapolated average temperature *extra* $\overline{T_{cold}}$ for the cold particles is also evaluated. More quantitative comparisons are presented in order to compare the standard to the extrapolated DEM. To do so, Voronoi diagram is used. It is a diagram that divides the region into smaller regions, the voronoi cells. The cells are generated based on a number of random points, the seeds. The data, temperature for this case, is affected to the closest seed forming the voronoi cell. As it can be seen in Figure 8 the system was divided into $v = 200$ voronoi cells and the error is calculated using the Equation 9 below:

$$\varepsilon_{rel} = \frac{1}{v} \frac{\sum_{i=1}^{v} |\overline{T_{DEM}}_{(i)} - \overline{T_{extra}}_{(i)}|}{|\overline{T_{hot}} - \overline{T_{cold}}|} = \frac{\varepsilon_{abs}}{|\overline{T_{hot}} - \overline{T_{cold}}|} \tag{9}$$

The physical meaning of the absolute error is that for 200 random cells, the average temperature of the particles $\overline{T_{DEM}}$ in a random cell for the DEM is

Table 5: Absolute and relative errors per extrapolation step.

Extrapolation step	t_2	t_3	t_4	t_5	t_6	t_7
ε_{abs} (K)	0.241	0.126	0.083	0.062	0.042	0.03
ε_{rel} (%)	1.84	1.275	1.27	1.69	2.25	3.09

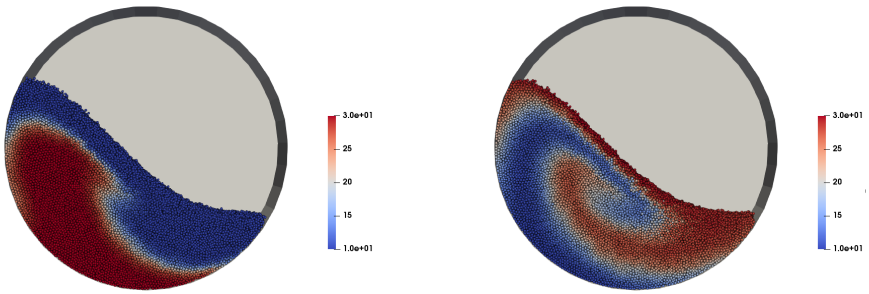

t_0 t_1

(a) (b)

Figure 4: Initial configuration for pairing algorithm.

compared with the extrapolated average temperature of the particles $\overline{T_{extra}}$ in the same cell and the sum of the difference of those temperature over the number of cells is calculated. The maximum absolute error is of order of 0.2 Kelvin which is small. Furthermore, the relative error is obtained by dividing the absolute error by the difference of the DEM $\overline{T_{hot}}$ and DEM $\overline{T_{cold}}$. The maximum relative error is also smaller than 3% which is considered as an acceptable error as shown in Table 5. This implies that the method is efficient and reliable. It is to be noted that the Figure 7 represents a temporal comparison for the results whereas the Figure 8 stands for the spacial comparison.

As we can visualize, the extrapolated findings of DEM represents a realistic reproduction of the results of standard DEM with a significant reduction of the

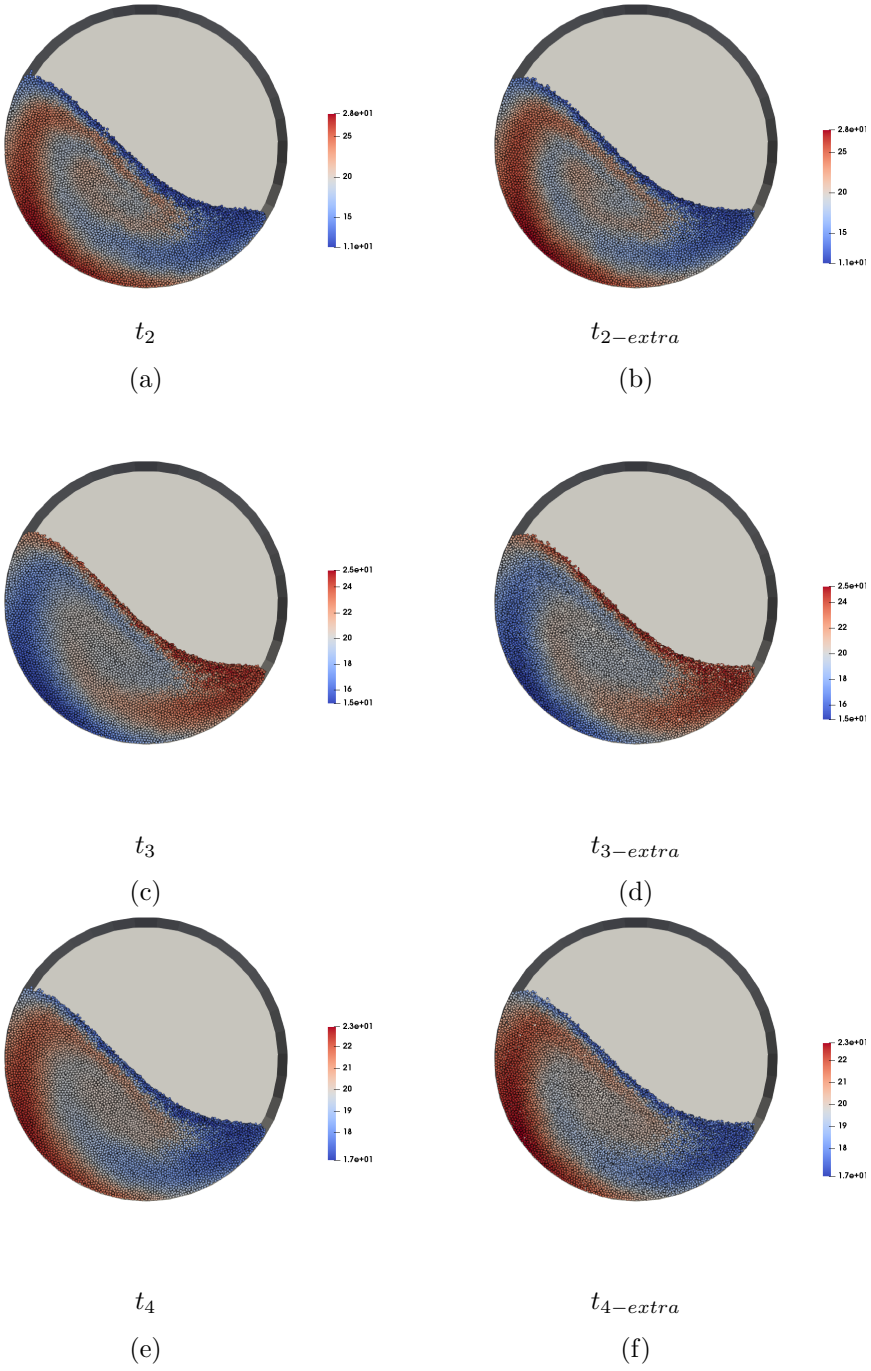

t_2 (a) $t_{2-extra}$ (b)

t_3 (c) $t_{3-extra}$ (d)

t_4 (e) $t_{4-extra}$ (f)

Figure 5: Comparison between standard and extrapolated DEM.

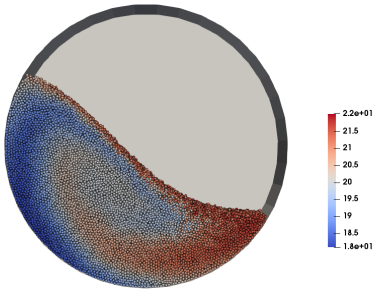

t_5

(g)

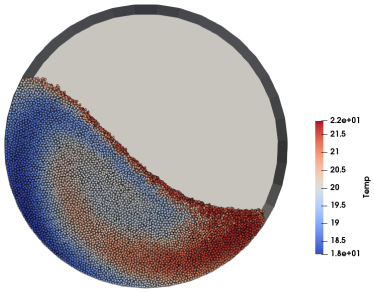

$t_{5-extra}$

(h)

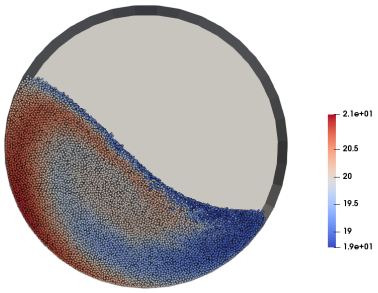

t_6

(i)

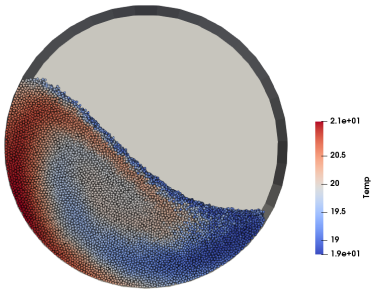

$t_{6-extra}$

(j)

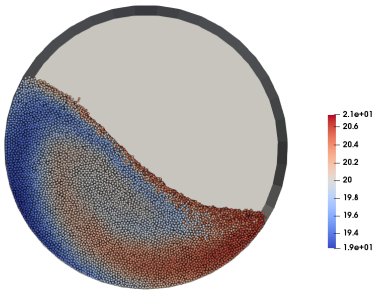

t_7

(k)

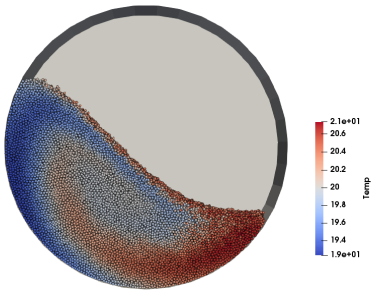

$t_{7-extra}$

(l)

Figure 6: Comparison between standard and extrapolated DEM.

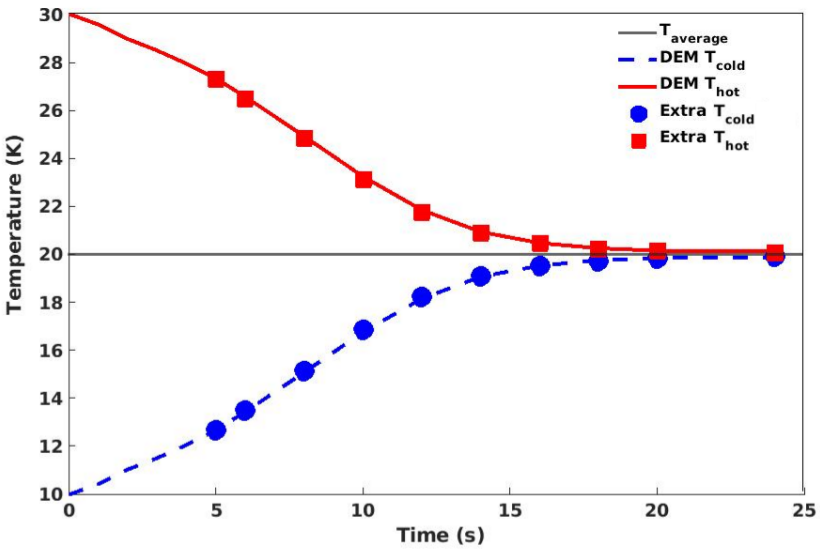

Figure 7: Comparison between DEM results with extrapolated DEM results for heat transfer for the reference case.

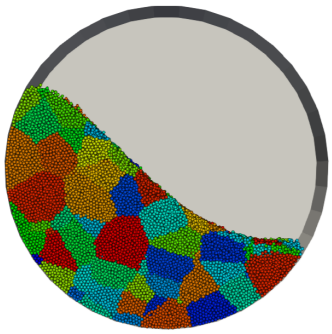

Figure 8: Repartition of 200 voronoi cells in the rotating drum for the study of efficiency.

Table 6: Simulations Performance for 100 τ of real time.

Case	Complete DEM	Extrapolated DEM
80000 particles		
Until t_1 (s)	8580	8580
Pairing (s)	0	551
Collision file (s)	0	7619
For one τ (s)	3900	6
Total simulation time for 100 τ(s)	398580	17350

computational time. All the simulations ran over the cluster centaure of **Mines Saint-Etienne** with one node (one thread only) at 2.66 GHz to evenly compare the computational time. Since they require high RAM[9] , the node that was used is equipped with big memory that consits of 500 Gb. The extrapolated DEM requires a CPU of just 6 seconds/ τ whereas the standard DEM takes a CPU of 3900 seconds/ τ as in Table 6. This method is efficient if the results required are for longer industrial time. The reduction of the CPU is of an order of 650 per τ while illustrating accurately the results. The computational time can be changed by modifying other parameters and this will be presented in the next sections.

3.2. Influence of the sampling parameters

The new method presented is really promising in terms of the gain of the computational time and rapidity of the simulation. But it requires a high use of RAM due the obligation of saving the microscopic characteristic of the particles as m and the $\sqrt{(a_{ij})}$ of collisions. Therefore, to solve the latter problem and to reduce the computational time more, statistical approaches are done. These approaches study the effect of the parameter affecting the temperature evolution as shown in Equation 5. The temperature term is proportional to the multipli-

[9]Random Access Memory

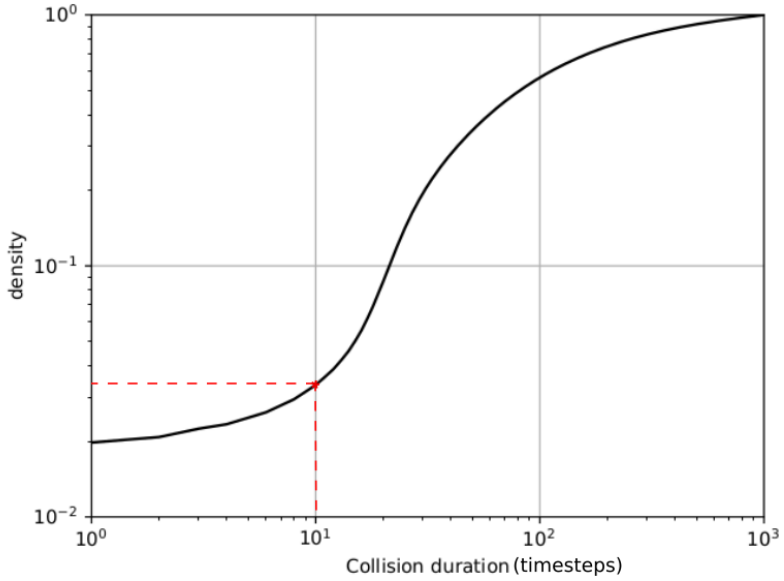

Figure 9: Cumulated density function for collision occurrence.

cation of m and the $\sqrt{(a_{ij})}$ of the particles. Therefore, the statistics show the density of the collisions duration or how much time does the majority of the collision lasts. The graph output's can explicit if the omission of small duration collision will affect highly the results or not. According to Figure 9, n can be deduced. For this case, 97% of the collisions lasts more than 10 timesteps. This enables saving every $n = 10$ timesteps instead of every one timestep. Indeed the results will be affected a little bit, but this can be explained by not aiming for exact results instead for acceptable, fast and low cost results. Thus, the extrapolated heat transfer results are expected to loose about 3 % in comparison with the normal DEM simulations' values since the collisions with $\Delta t_c < 10\Delta t_{DEM}$ seconds will be neglected due to collision sampling as in Figure 9.

To study the impact of the sampling parameters on the results, n and Δt_c^{max} were modified. The Figure 10 shows the percentage error for the energy transferred from t_n to t_{n+1} in standard DEM in comparison with the energy transferred from t_n to t_{n+1} in extrapolated DEM as in Equation 10. This will show

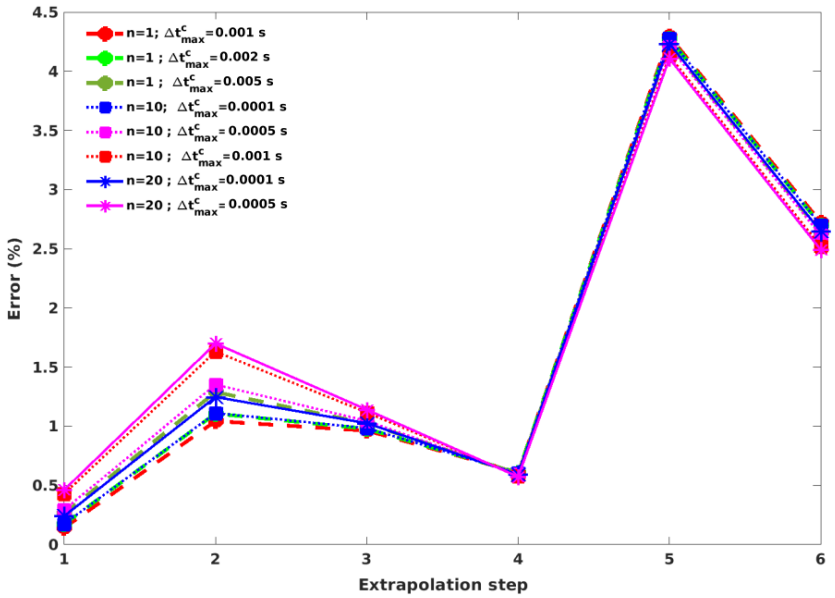

Figure 10: Percentage error for different sampling parameters with saving every n timesteps and each collision lasts a maximum of Δt_c seconds.

if the transfer for the extrapolated DEM is reliable.

$$\varepsilon = \frac{\sum(|T_{n+1} - T_n|) - \sum(|T_{n+1-extra} - T_{n-extra}|)}{\sum(|T_{n+1} - T_n|)} \tag{10}$$

The difference between the results is not significant. The errors varies between 0.1 % and 4.5% as in Figure 10. The scenario that will be used for further studies is that of $n = 10$ and $m = 10$ since it has the least computational time with reasonable results.

3.3. Influence of the setup parameters

Several setup parameters can be changed to evaluate the results. Some of them are: the number of particles, the initial condition (adiabatic wall or not)), the rotating velocity of the drum that affect the regime inside the drum and the pairing period (half rotation or full rotation) and etc...This analysis is presented below.

Table 7: Testing several particles number.

Case	Complete DEM	Extrapolated DEM
400000 particles		
Until t_1 (s)	25620	25620
Pairing (s)	0	3060
Collision file (s)	0	19680
For one τ (s)	4860	24
Total simulation time for 100 τ(s)	493620	50760

3.3.1. The number of particles

The DEM simulations were performed for different particles' number inside the rotating drum. Many cases were simulated. The following section will present another scenario with 400000 particles. All the physical parameters chosen are the same as of those in the reference case, it is only the number of particles packed that changes. Here, $n = 1$ and τ is taken to be 0.1ω instead of 0.5ω as in the reference case since we are limited with the memory. It should be noted that the higher the number of particles, the more the method is efficient and the bigger the gain in the computational time Table 7. Also, if the particle's number increases the CPU time increases as well. However, for the extrapolated simulation, the pairing method is efficient when bigger system is employed as in Bednarek et al. (2019). Then the time for the creation of the collision file can be minimized easily by using the sampling; and finally each extrapolation step takes no more than a minute.

3.3.2. Regimes in rotating drum

An analysis for the previously described method is performed for different regimes in the rotary drum. Six different regimes can identified in the rotary drum. These regimes depend on a dimensionless group known as Froude number which is proportional to the angular velocity of the drum and the percentage filling of the drum. This is explained in details by Mellmann (2001). By increas-

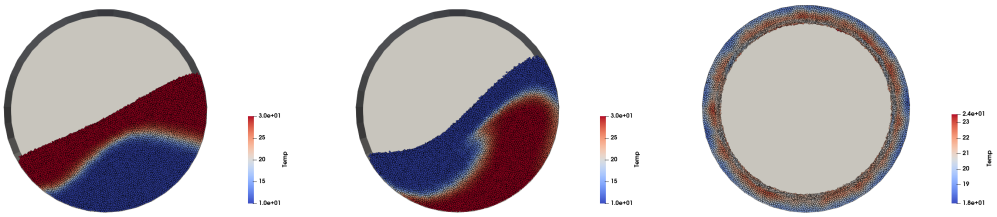

(a) (b) (c)

Figure 11: Different regimes used for the extrapolation case: (a) Rolling regime: 15 seconds/revolution; (b) Cascading regime: 5 seconds/revolution; (c) Centrifuging regime: 0.1 seconds/revolution.

ing or decreasing the angular velocity, the regimes can be visualized; the rolling regime Figure 11a takes 15 seconds per rotation, the cascading Figure 11b takes 5 seconds per rotation and finally the centrifuging Figure 11c takes 0.1 seconds per rotation. As shown in the sections before, the method is applied over a cascading regime, Figure 11b. To demonstrate that the used approach is general, it was tested over other regimes. The following results presented in Figure 12 shows the extrapolation for the rolling regime is possible. The extrapolation for Figure 11c was not performed since it does not present an interest specially because the particles do not have a relative movement. Hence, the method is an accurate description of what is happening with a drastic reduction of computational time. It should be mentioned that the proposed new method is general and may be used to a variety of pseudo-periodic granular systems.

3.3.3. The pairing period

The period for the pairing algorithm (initial time of period t_0 and initial extrapolation time t_1) is selected to be proportional to the time of the drum rotational speed ω, i.e. $\alpha * \omega$ is equal to 0.1ω, 0.5ω, 1ω, 2ω, etc...

Various extrapolation periods were studied; quarter rotation, half rotation and full rotation. In the previous section, results for full rotation's extrapolation were evoked and in this section we will present different τ values. Figure 14 shows extrapolating every quarter turn and Figure 15 for half rotation extrap-

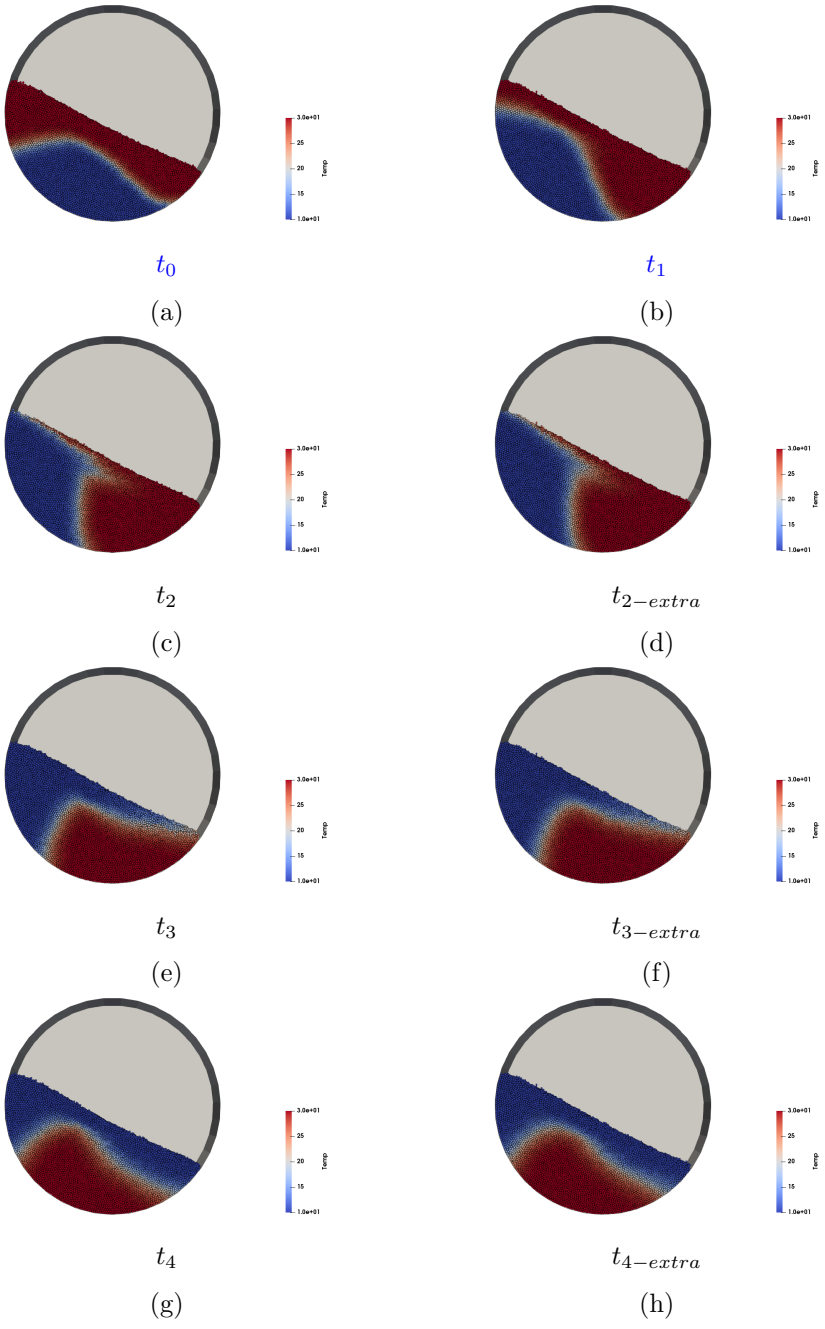

Figure 12: Extrapolation for the rolling regime.

olation. The method works effectively in all scenarios used as it can be seen in Figure 13 describing the evolution of the temperature with the change of α a constant proportional to the pairing period.

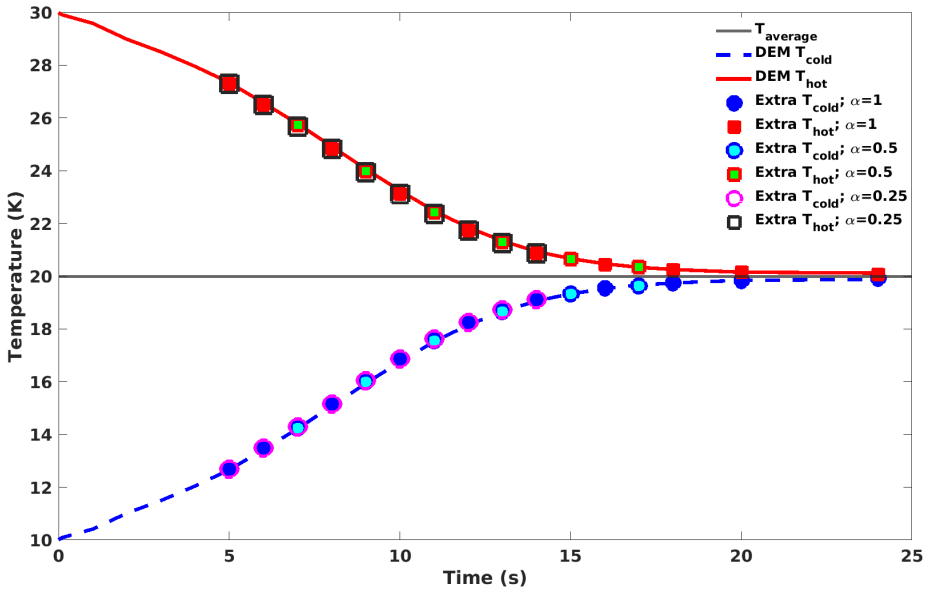

Figure 13: Comparison between DEM results and extrapolated DEM results for heat transfer changing α for different pairing period.

It should be also noted that the bigger the extrapolation time, the bigger the output file, the higher the RAM used and the lower the computational time. It is always a compromise between the computational time and the RAM. In order to use higher extrapolation period with an acceptable memory usage, the sampling should be higher, i.e. saving every 10 or 20 timesteps. Also, the speed of the extrapolation is linked to the parameter alpha (the difference between t_0 and t_1). Hence if the objective is to find what is happening for very long time in the simulation, higher value of alpha will give the required results faster. This can be seen in following comparative Table 8.

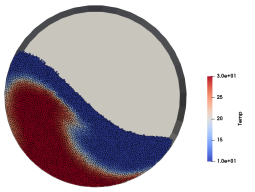

t_0

(a)

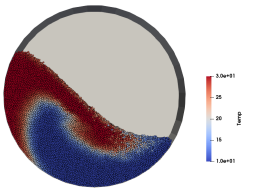

t_1

(b)

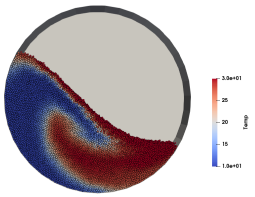

t_2

(c)

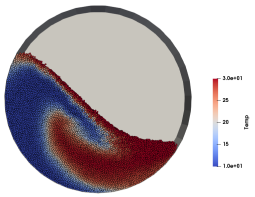

$t_{2-extra}$

(d)

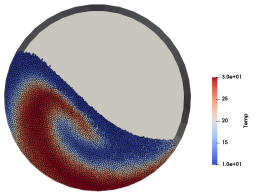

t_3

(e)

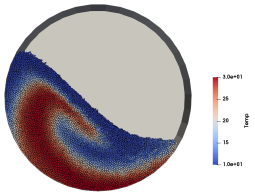

$t_{3-extra}$

(f)

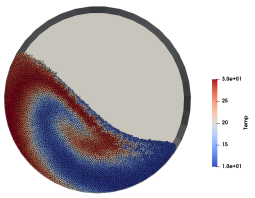

t_4

(g)

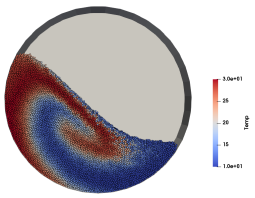

$t_{4-extra}$

(h)

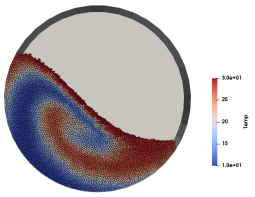

t_5

(i)

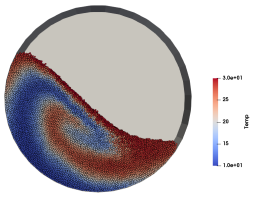

$t_{5-extra}$

(j)

Figure 14: Extrapolation every quarter rotation.

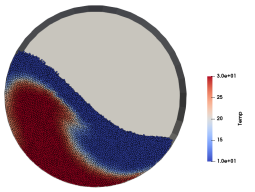

t_0

(a)

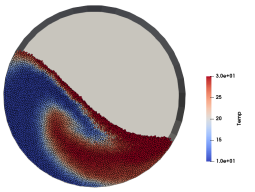

t_1

(b)

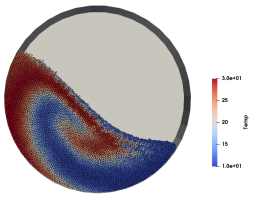

t_2

(c)

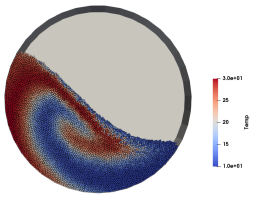

$t_{2-extra}$

(d)

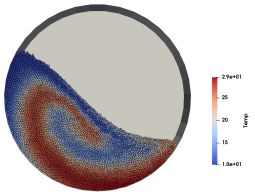

t_3

(e)

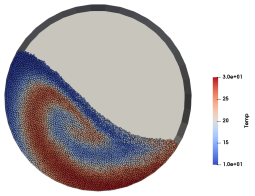

$t_{3-extra}$

(f)

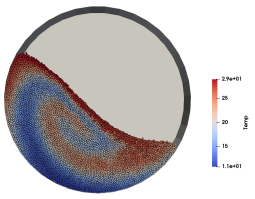

t_4

(g)

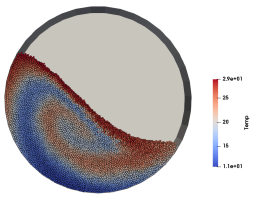

$t_{4-extra}$

(h)

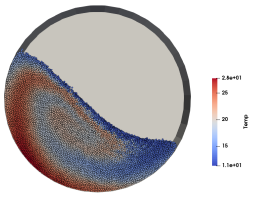

t_5

(i)

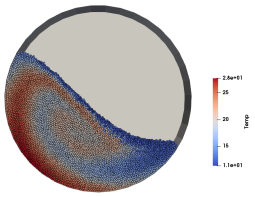

$t_{5-extra}$

(j)

Figure 15: Extrapolation every half rotation.

Table 8: Comparative table for different pairing period with $n = 10$ and $\Delta t_c^{max} = 10$.

Extrapolation period	Collision file size (Mb)	Time for one rotation(s)
quarter rotation	560	13
half rotation	1200	12
full rotation	2800	10

4. Conclusion

To understand the behavior of heat transfer due to particle-particle interactions in dry granular media, DEM simulations were performed. Those simulations require high computational time indicating the potency of developing new methods to speed them up. The newly developed algorithm has proved its efficacy and precision with a low computational time and cost. The results obtained show that from one period of DEM simulations, information for longer periods can be revealed. The extrapolated findings agree with the complete simulation results with less than 3% error and with a computational gain factor of more than 100. This work is promising and serves as a foundation for future researches on the topic as the extrapolation for a coupled granular flow simulation using CFD-DEM while taking into account the influence of the interstitial fluid (convective heat transfer).

Acronyms

CFD Computational Fluid Dynamics 3, 30

CFL Courant Friedrichs Lewy 11

CPU Central Processing Unit 3, 21, 24

DEM Discrete Element Method 1–8, 10, 11, 16, 17, 21–24, 30

FEM Finite Element Method 2

LIGGGHTS LAMMPS Improved for General Granular and Granular Heat Transfer Simulations 5

RAM Random Access Memory 21, 27

SPH Smoothed Particle Hydrodynamics 3

TDEM Thermal Discrete Element Method 2

Nomenclature

A_p Particle's cross sectional area (m^2) 6

ε_{abs} Absolute error 16, 17

α Constant 25, 27

a_{ij} Contact area (m^2) 5–7, 9, 11, 21, 22

$Biot^*$ Quasi-Biot number for particle–particle conduction 6

C_i Particle's specific thermal capacity J/(Kg.K) 6, 11, 13, 15

Δt_c Real Collision Duration (s) 9, 10, 22, 23

$\Delta t_{critical}$ Critical duration (s) 13

Δt_{DEM} DEM timestep (s) 22

ε Error 23

H_{ij} Conductance between the particles (K/W) 5

i Particle i 5–7, 9, 11, 13

j Particle j 5–7, 9, 11, 13

k Particle k 13

K_i Thermal conductivity of particle i W/(K.m) 5

K_{ij} Thermal conductivity W/(K.m) 5, 6, 11, 15

K_j Thermal conductivity of particle j W/(K.m) 5

l Particle l 13

m Duration of a single collision in seconds 9–11, 13, 21–23

n Sampling factor 9, 16, 22–24, 30

ω Rotational speed (s/revolution) 15, 24, 25

Δ_n Overlap distance of two particles (m) 6

$\vec{x}$ Position vector for DEM particles 7

Q_i Particle's heat flux (W) 6

Q_{ij} Heat flux due to particle-particle collision (W) 5, 13

r^* Mean particle radii (m) 15

r_c Contact radius between two particles (m) 6

r_p Particle radius (m) 6

ε_{rel} Relative error 16, 17

ρ Particle's density (Kg/m^3) 6, 11, 13, 15

f_{ext} Extrapolation function 7, 10, 13

T Temperature (K) 15

t_0 First instant of the extrapolation period (s) 8–10, 12, 16, 17, 25–29

t_1 Final instant of the extrapolation period (s) 7–10, 12, 16, 17, 21, 24–29

t_2 Instant of the first extrapolation step (s) 7, 11, 12

Δt_c^{max} Imposed maximum collision duration (s) 8–10, 16, 22, 30

$\overline{T_{cold}}$ Average temperature of the cold particles (K) 16, 17

$\overline{T_{DEM}}$ Average temperature of the particles for the DEM results (K) 16

$\overline{T_{extra}}$ Average temperature of the particles for the extrapolated results (K) 16, 17

$\overline{T_{hot}}$ Average temperature of the hot particles (K) 16, 17

t_{init} Initial time (s) 9, 14

t_{max} Maximum collision duration (s) 5

τ Extrapolation period 16, 21, 24, 25

T_i Temperature of the particle i (K) 5, 6, 13

T_j Temperature of the particle j (K) 5, 6, 13

v Number of voronoi cells 16

V_i Particle's volume (m^3) 6, 11, 13

References

Bauer, H., Matić, J., Evans, R. C., Gryczke, A., Ketterhagen, S. K., W., & Khinast, J. (2022). Determining local residence time distributions in twin-screw extruder elements via smoothed particle hydrodynamics. *Chemical Engineering Science*, *247*, 117029.

Beaulieu, C., Vidal, D., Yari, B., Chaouki, J., & Bertrand, F. (2021). Impact of surface roughness on heat transfer through spherical particle packed beds. *Chemical Engineering Science*, *231*, 116256.

Bednarek, X., Martin, S., Ndiaye, A., Peres, V., & Bonnefoy, O. (2019). Extrapolation of dem simulations to large time scale. application to the mixing of powder in a conical screw mixer. *Chemical Engineering Science*, *197*, 223–234.

Bertrand, F., Leclaire, L. A., & Levecque, G. (2005). Dem-based models for the mixing of granular materials. *Chemical Engineering Science*, *60*, 2517–2531.

Chaudhuri, B., Muzzio, F., & Tomassone, M. (2006). Modeling of heat transfer in granular flow in rotating vessels. *Chemical Engineering Science*, *61*, 6348 – 6360. doi:https://doi.org/10.1016/j.ces.2006.05.034.

Cundall, P., & Strack, O. D. (1979). A discrete numerical model for granular assemblies. *Geotechnique*, *29*, 47–65.

De, T., Chakraborty, J., Kumar, J., Tripathi, A., Sen, M., & Ketterhagen, W. (2022). A particle location based multi-level coarse-graining technique for discrete element method (dem) simulation. *Powder Technology*, *398*, 117058.

Doucet, J., Hudon, N., Bertrand, F., & Chaouki, J. (2008). Modeling of the mixing of monodisperse particles using a stationary dem-based markov process. *Computers & Chemical Engineering*, *32*, 1334–1341.

Feng, Y., Han, K., Li, C., & Owen, D. (2008). Discrete thermal element modelling of heat conduction in particle systems: Basic formulations. *Journal of Computational Physics*, *227*, 5072–5089.

Feng, Y., Han, K., & Owen, D. (2009). Discrete thermal element modelling of heat conduction in particle systems: pipe-network model and transient analysis. *Powder Technology*, *193*, 248–256.

Fry, A. M., Umbanhowar, P. B., Ottino, J. M., & Lueptow, R. M. (2019). Diffusion, mixing, and segregation in confined granular flows. *AIChE Journal*, *65*, 875–881.

Gui, N., Yan, J., Xu, W., Ge, L., Wu, D., Ji, Z., Gao, J., Jiang, S., & Yang, X. (2013). Dem simulation and analysis of particle mixing and heat conduction in a rotating drum. *Chemical Engineering Science*, *97*, 225–234.

Hartmanshenn, C., Khinast., J., Papageorgiou, C., Mitchell, C., Quon, J., & Glasser, B. (2019). Heat transfer of dry granular materials in a bladed mixer: Effect of thermal properties and agitation rate. *AIChE Journal*, *66*. doi:https://doi.org/10.1002/aic.16861.

Herz, F., Mitov, I., Specht, E., & Stanev, R. (2012). Influence of operational parameters and material properties on the contact heat transfer in rotary kilns. *International Journal of Heat and Mass Transfer*, *55*, 7941–7948.

Huang, A., & Kuo, H. (2018). Cfd simulation of particle segregation in a rotating drum. *Advanced Powder Technology*, *29*, 3368–3374. doi:https://doi.org/10.1016/j.apt.2018.09.019.

Kiani-Oshtorjani, M., & Jalali, P. (2019). Thermal discrete element method for transient heat conduction in granular packing under compressive forces. *International Journal of Heat and Mass Transfer*, *145*, 118753.

Kiani-Oshtorjani, M., Kiani-Oshtorjani, M., Mikkola, A., & Jalali, P. (2022). Conjugate heat transfer in isolated granular clusters with interstitial fluid using lattice boltzmann method. *International Journal of Heat and Mass Transfer*, *187*, 122539.

Kloss, C., Goniva, C., Hager, A., Amberger, S., & Pirker, S. (2012). Models, algorithms and validation for opensource dem and cfd-dem. *Progress in Computational Fluid Dynamics, An International Journal*, *12*, 140.

Lichtenegger, T. (2020). Fast eulerian-lagrangian simulations of moving particle beds under pseudo-steady-state conditions. *Powder Technology*, *362*, 474 – 485. URL: http://www.sciencedirect.com/science/article/pii/S0032591019309428. doi:https://doi.org/10.1016/j.powtec.2019.10.113.

Lichtenegger, T., Kieckhefen, P., Heinrich, S., & Pirker, S. (2019). Dynamics and long-time behavior of gas–solid flows on recurrent-transient backgrounds. *Chemical Engineering Journal*, *364*, 562 – 577. URL: http://www.sciencedirect.com/science/article/pii/S1385894719301792. doi:https://doi.org/10.1016/j.cej.2019.01.161.

Lichtenegger, T., Peters, E., Kuipers, J., & Pirker, S. (2016). A recurrence cfd study of heat transfer in a fluidized bed. *Chemical Engineering Journal*, *172*, 310 – 322.

Lichtenegger, T., & Pirker, S. (2016). Recurrence cfd–a novel approach to simulate multiphase flows with strongly separated time scales. *Chemical Engineering Journal*, *153*, 394 – 410.

Liu, X., Gui, N., Yang, X., Tu, J., & Jiang, S. (2021). A new discrete element-embedded finite element method for transient deformation, movement and heat transfer in packed bed. *International Journal of Heat and Mass Transfer*, *165*, 120714.

Mellmann, J. (2001). The transverse motion of solids in rotating cylinders—forms of motion and transition behavior. *Powder Technology*, *118*, 251–270.

Muzzio, F., Alexander, A., Goodridge, C., Shen, E., Shinbrot, T., Manjunath, K., & Jacob, K. (2004). Solids mixing. *Handbook of Industrial Mixing*, (p. 887–985). doi:https://doi.org/10.1002/0471451452.ch15.

Nguyen, H. T., Cosson, B., Lacrampe, M. F., & Krawczak, P. (2014). Numerical simulation on the flow and heat transfer of polymer powder in rotational molding. *International Journal of Material Forming*, *8*, 423–438.

Peng, Z., Doroodchi, E., & Moghtaderi, B. (2020). Heat transfer modelling in discrete element method (dem)-based simulations of thermal processes: Theory and model development. *Progress in Energy and Combustion Science*, *79*, 100847.

Peters, E., Kuipers, J. et al. (2023). A detailed gas-solid fluidized bed comparison study on cfd-dem coarse-graining techniques. *Chemical Engineering Science*, (p. 118441).

Pirker, S., & Lichtenegger, T. (2018). Efficient time-extrapolation of single- and multiphase simulations by transport based recurrence cfd (rcfd). *Chemical Engineering Science*, *188*, 65 – 83. URL: http://www.sciencedirect.com/science/article/pii/S0009250918302732. doi:https://doi.org/10.1016/j.ces.2018.04.059.

Saruwatari, M., & Nakamura, H. (2022). Coarse-grained discrete element method of particle behavior and heat transfer in a rotary kiln. *Chemical Engineering Journal*, *428*, 130969.

Siegmann, E., Enzinger, S., Toson, P., Doshi, P., Khinast, J., & Jajcevic, D. (2021). Massively speeding up dem simulations of continuous processes using a dem extrapolation. *Powder Technology*, *390*, 442–455.

Vargas, W. L., & McCarthy, J. J. (2001). Heat conduction in granular materials. *Aiche Journal*, *47*, 1052–1059.

Wang, S., Luo, K., Hu, C., Lin, J., & Fan, J. (2019). Cfd-dem simulation of heat transfer in fluidized beds: Model verification, validation, and application. *Chemical Engineering Science*, *197*, 280–295.

Yazdani, E., & Hashemabadi, S. (2020). Three-dimensional heat transfer in a particulate bed in a rotary drum studied via the discrete element method. *Particuology*, *51*, 155–162.

Zhang, H., Zhou, Q., & Zheng, Y. (2011). A multi-scale method for thermal conduction simulation in granular materials. *Computational materials science*, *50*, 2750–2758.

Zhao, S., Zhao, J., & Lai, Y. (2020). Multiscale modeling of thermo-mechanical responses of granular materials: A hierarchical continuum–discrete coupling

approach. *Computer Methods in Applied Mechanics and Engineering*, *367*, 113100.

Zhu, H., Zhou, Z., Yang, R., & Yu, A. (2007). Discrete particle simulation of particulate systems: theoretical developments. *Chemical Engineering Science*, *62*, 3378–3396.